HHS Public Access

Author manuscript

ACS Appl Mater Interfaces. Author manuscript; available in PMC 2022 May 09.

Published in final edited form as:

ACS Appl Mater Interfaces. 2020 November 11; 12(45): 50222–50235. doi:10.1021/acsami.0c13304.

Modifying Cell Membranes with Anionic Polymer Amphiphiles Potentiates Intracellular Delivery of Cationic Peptides

Eric A. Dailing,
Department of Biomedical Engineering, Vanderbilt University, Nashville, Tennessee 37235, United States

Kameron V. Kilchrist,
Department of Biomedical Engineering, Vanderbilt University, Nashville, Tennessee 37235, United States

J. William Tierney,
Department of Biomedical Engineering, Vanderbilt University, Nashville, Tennessee 37235, United States

R. Brock Fletcher,
Department of Biomedical Engineering, Vanderbilt University, Nashville, Tennessee 37235, United States

Brian C. Evans,
Department of Biomedical Engineering, Vanderbilt University, Nashville, Tennessee 37235, United States

Craig L. Duvall
Department of Biomedical Engineering, Vanderbilt University, Nashville, Tennessee 37235, United States

Abstract

Rapid, facile, and noncovalent cell membrane modification with alkyl-grafted anionic polymers was sought as an approach to enhance intracellular delivery and bioactivity of cationic peptides. We synthesized a library of acrylic acid-based copolymers containing varying amounts of an amine-reactive pentafluorophenyl acrylate monomer followed by postpolymerization modification with a series of alkyl amines to afford precise control over the length and density of aliphatic

Corresponding Author craig.duvall@vanderbilt.edu.

The authors declare no competing financial interest.

ASSOCIATED CONTENT

Supporting Information

The Supporting Information is available free of charge at https://pubs.acs.org/doi/10.1021/acsami.0c13304.
NMR spectra; gel permeation chromatography results; red blood cell hemolysis results; polymer cytotoxicity; confocal microscopy images; polymer intracellular uptake; Nile Red fluorescence intensity; confocal zslices of polymer-treated A7r5 cells; polymer and peptide uptake in the presence of endocytosis inhibitors; schematic of MK2i-mediated inhibition of luciferase expression following PDGF stimulation; validation of luminescence in CREB-luc positive A7r5 cells; map of the plasmid used to generate the HEK 293-T LgBiT cell line; validation of luminescence in LgBiT-positive HEK-293T cells; fold change in luminescence in LgBiT-positive cells following pyrene butyrate treatment; and pyrene butyrate cytotoxicity (Figures S1–S30), concentrations at which the linear fits from the Nile red assay intersect; and the amino acid sequence of reported cell penetrating sequences and net charge of CPPMK2i and CPP-HiBiT (Tables S1–S2), supplemental discussion, and references S1–3 (PDF).

alkyl side chains. This synthetic strategy enabled systematic investigation of the effect of the polymer structure on membrane binding, potentiation of peptide cell uptake, pH-dependent disruption of lipid bilayers for endosome escape, and intracellular bioavailability. A subset of these polymers exhibited pK_a of ~6.8, which facilitated stable membrane association at physiological pH and rapid, pH-dependent endosomal disruption upon endocytosis as quantified in Galectin-8-YFP reporter cells. Cationic cell penetrating peptide (CPP) uptake was enhanced up to 15-fold in vascular smooth muscle cells in vitro when peptide treatment was preceded by a 30-min pretreatment with lead candidate polymers. We also designed and implemented a new and highly sensitive assay for measuring the intracellular bioavailability of CPPs based on the NanoLuciferase (NanoLuc) technology previously developed for measuring intracellular protein–protein interactions. Using this split luciferase class of assay, polymer pretreatment enhanced intracellular delivery of the CPP-modified HiBiT peptide up to 30-fold relative to CPP-HiBiT without polymer pretreatment ($p < 0.05$). The overall structural analyses show that polymers containing 50:50 or 70:30 molar ratios of carboxyl groups to alkyl side chains of 6–8 carbons maximized peptide uptake, pH-dependent membrane disruption, and intracellular bioavailability and that this potentiation effect was maximized by pairing with CPPs with high cationic charge density. These results demonstrate a rapid, mild method for polymer modification of cell surfaces to potentiate intracellular delivery, endosome escape, and bioactivity of cationic peptides.

Graphical Abstract

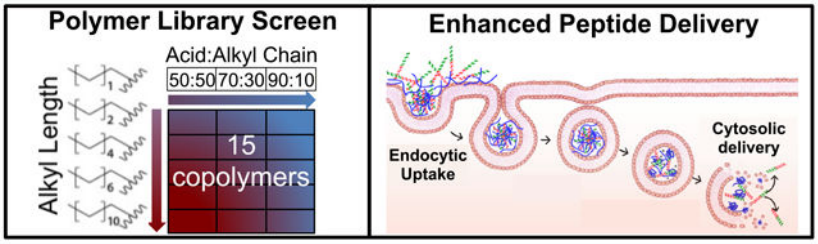

Keywords

RAFT polymers; peptides; drug delivery; endosomal escape; cell surface modification

INTRODUCTION

Polymer-based cell surface modification is a versatile technique that can be used to improve the efficacy of cell-based applications in tissue engineering, drug delivery, and immunotherapy by introducing chemical functionalities onto the cell membrane that provide handles for cell surface binding of bioactive compounds or modulate cell–cell interactions.[1–5] The most commonly used state of the art for polymer modification of the cell surface involves electrostatic deposition of cationic polymers onto negatively charged cell membranes. The plasma membrane supports stable complexation with amine-containing polymers such as poly(l-lysine), poly(ethyleneimine), or poly(allylamine), enabling the introduction of bioorthogonal functional groups[6] or layer-by-layer coating with polyanions, an approach that has been explored for pancreatic islet encapsulation to improve transplant survival.[7–9] Cationic polymer precoating has also been used to increase viral transfection

efficiency, with polybrene and protamine sulfate commonly applied to facilitate cell membrane interaction with anionic viral envelopes.[10,11] In contrast, coating of noncationic polymers onto cell surfaces requires polymers that insert into the cell membrane lipid bilayer through hydrophobic functionalities. For example, polyvinyl alcohol (PVA) and poly(ethylene glycol) (PEG)-based amphiphiles with single lipid chain-end modifications anchored to pancreatic islet surfaces are able to improve transplant survival by passively shielding the graft against host immune reactions[12,13] or by serving as handles for immobilizing bioactive proteins that attenuate adverse thrombogenic events.[14] Bertozzi and co-authors extended this polymer-based cell modification approach toward the generation of synthetic mucin-mimetic glycopolymers containing membrane-anchoring lipids. These polymers stably associated into cell membranes to display glycans that direct cell-surface biochemical interactions such as molecular recognition by carbohydrate-binding proteins and adhesion to the extracellular matrix.[15,16]

In this report, we describe a new application of noncovalent cell surface-modifying polymers to promote uptake and cytosolic delivery of intracellularly active peptides. Peptides are powerful tools for potent and specific modulation of intracellular protein–protein interactions and signaling pathways. However, peptides have limited cytosolic bioavailability due to poor cellular uptake and retention, endosomal vesicle entrapment, exocytosis through recycling endosomes, and degradation within lysosomes.[17,18] Peptides are frequently modified with cationic "cell penetrating" sequences designed to facilitate cell uptake, but these sequences generally do not drive robust uptake or escape from endosomal and lysosomal compartments. Cyclic cell-penetrating peptides (CPPs) have shown some promise toward cytosolic delivery, but the synthesis and covalent attachment to the payload of interest are complex and inefficient.[19–21] Cellular pretreatment with the small molecule pyrene butyrate has been investigated for facilitating membrane translocation of cationic peptides, but its application is generally limited to oligoarginine CPPs andhas no demonstrated endosome disrupting behavior.[22–24]

Here, we sought an approach to drive cationic peptide uptake and intracellular bioavailability through a polymer-based approach that is potentially applicable to a variety of cell and tissue types. Antibodies and other receptor targeting ligands have broad application for site-specific delivery following systemic administration or regional retention in locally administered formulations and are effective toward intracellular delivery of bioactive macromolecules such as enzymes.[25–30] In contrast to these more selective platforms, nontargeted polymer pretreatment is potentially more universal and represents a low-cost, highly scalable alternative to antibody conjugation. We envision clinical applications of this delivery technology to primarily include topical delivery to cell therapies, engineered tissues, or explanted allogeneic or autologous tissues prior to implant in vivo. As examples, our previous work has demonstrated both in vitro and ex vivo polymer-based delivery strategies for enhancing peptide bioactivity in cells and vascular tissue.[31,32] Though underexplored to this point, in vivo topical or local delivery, such as into a skin wound bed, articular joint space, or arterial vessel wall using catheter-based technologies,[33] is also anticipated to be feasible implementations of this technology.

In the current studies, we synthesized and screened cell surface-modifying polymers that consider the parallel design goals of both driving robust peptide uptake and facilitating escape from intracellular endolysosomal vesicles. Few studies specifically detail the optimization of polymeric delivery reagents for cationic peptides, and none to our knowledge focuses on optimizing hydrophobe length and density for cell surface modification to potentiate intracellular peptide delivery. To bridge this gap, we evaluated a library of anionic polymers containing multivalent hydrophobic modifications with the goal of identifying candidates that would (1) anchor onto and coat cell surfaces without affecting cell viability, (2) contribute negative surface charge to increase the electrostatic attraction and internalization of cationic peptides, and (3) have appropriately tuned the acid dissociation constant, or pK_a, such that the polymer has protonation-dependent solubility, becoming hydrophobic to facilitate membrane interaction/disruption in the acidic pH range encountered during endolysosomal trafficking while remaining inert at physiologic pH.

We hypothesized that the ideal candidate polymer for this approach will contain sufficient negative charge density through acid groups that "bait" the cationic peptide and concentrate it at the cell membrane at extracellular pH. However, because the cell membrane is negatively charged, we posited that multivalent interactions between the cell membrane and alkyl hydrophobic anchors of optimized density and length would be required to overcome the electrostatic repulsion between an anionic polymer and the cell surface to achieve efficient coating while avoiding cell membrane lysis or cytotoxicity. Additional design complexity arises from the impact that hydrophobic groups have on polymer pK_a and the goal of tuning the polymer to have a pH-dependent solubility switch in the endosomal pH range. With these considerations in mind, we sought to synthesize a series of well-defined polymers with a range of densities of carboxylic acids and hydrophobic alkyl grafts of varied length.

RESULTS AND DISCUSSION

To generate a polymer library, a series of random copolymer "parent polymers" containing different molar ratios of t-butyl acrylate (tBA) and pentafluorophenyl acrylate (PFPA) were first prepared via reversible addition–fragmentation chain transfer (RAFT) polymerization (Scheme 1A). PFPA contains an amine-reactive ester and has previously been reported as a robust functional group for preparing polymers with diverse structures[34–36] because postpolymerization modification with primary amines occurs rapidly and quantitatively in polar, aprotic solvents in ambient conditions.[37]

In this study, we applied PFPA to facilitate facile postpolymerization modification with varied aliphatic alkyl amines. This ‘conjugation-to’ approach was chosen to ensure that, within a given alkyl chain density series, the resultant polymers are compositionally identical with the exception of the alkyl graft length. While it is possible to prepare these polymers directly from acrylic acid and different alkyl acrylates or acrylamides, compositional drift due to varying monomer reactivity ratios may complicate directly comparing the effects of alkyl chain length for a given monomer composition. After the alkyl grafting step, cleavage of the t-butyl ester afforded a series of well-defined copolymers of acrylic acid and various alkyl acrylamides.

Using this synthetic approach, we prepared three initial copolymers with a 50:50, 70:30, or 90:10 ratio of tBA:PFPA, and each of these three parent polymers was then reacted in separate batches with five different alkyl amines to obtain a library of 15 copolymers (Scheme 1B). We selected these ratios and side chains in an effort to obtain a broad parameter space for rationally interrogating cell surface modification and pH-dependent membrane-disrupting behavior with the ultimate goal to discover multiple water-soluble candidates that possess a pK_a that is optimal for endosome escape (6–6.8). We obtained good agreement between product composition and monomer feed ratios via ^{1}H NMR (Figures S1–16), and polymers had comparable molecular weights and low polydispersity as determined by GPC (Table 1 and Figure S17). Amine grafting and t-butyl ester cleavage proceeded to >99% conversion in ambient conditions as determined via ^{19}F and ^{1}H NMR, respectively, confirming that our synthetic approach provides a robust, modular strategy for generating polymers with a well-defined structure and chemical composition.

Ideally tuned polymers with the appropriate pK_a and level of hydrophobicity will safely coat cell surfaces at pH 7.4 yet destabilize endosomal membranes through a pH-dependent coil-to-globule transition at acidic pH.[38] The pH transition depends on polymer pK_a,[39] which we sought to tune through precise control of polymer hydrophobicity. The pK_a of each polymer in our library was measured via acid–base titration (Figure 1A) in which each polymer was prepared as the sodium salt and titrated to the acidic endpoint. Previous reports have demonstrated that increasing polymer hydrophobicity reduces the relative degree of ionization at a given equilibrium pH, manifesting in a higher pK_a.[40,41] Intramolecular charge repulsion dominates in highly ionized polymers, while hydrophobic interactions become increasingly significant as carboxylate ions are protonated and can directly affect the dielectric constant around the remaining charged groups.[42,43]

We observed that polymer pK_a was invariant with alkyl chain length for the 90:10 copolymer composition, which suggests that a critical spatial proximity between hydrophobic side chains must be achieved to enable alteration of the pH-dependent protonation state. Indeed, a sharp increase in pK_a was observed for polymers containing >30 mol % alkyl side chains and particularly those with >6 carbons in the side chain. Four polymers exhibited pK_a values of 6.7–6.8 (50:50 AA:hexyl and AA:octyl, 70:30 AA:hexyl and AA:octyl), which is in the early endosomal pH range and which our previous reports identified as ideal for intracellular delivery with hydrophobic monomer-containing cationic copolymers.[44,45] Two polymers exhibited pK_a values >7.0 (50:50 and 70:30 AA:dodecyl), while the remaining polymers in our library had pK_a values <6.0, which falls within the late endosomal/lysosomal pH range.

We next screened all polymers in a red blood cell hemolysis assay to assess pH-dependent membrane disruption.[46] Polymers were incubated with isolated human red blood cells in isotonic solutions buffered to pH 7.4, 6.8, 6.2, or 5.6 to model physiological, early endosome, late endosome, and lysosomal environments, respectively. Polymer-mediated membrane lysis releases free hemoglobin, which is spectrophotometrically quantified relative to PBS and detergent negative and positive controls as percent hemolysis. No polymers induced observable hemolysis at physiological pH, but the subset of polymers with pK_a around 6.8 exhibited a switchlike, dose-dependent increase at or below pH 6.8

(Figure 1B, Figure S18). Our previous work indicated that membrane disruption at pH 6.8 is a strong predictor of polymeric reagents that will enhance intracellular bioavailabilty without significant cytotoxicity.[44,45,47] Tuning of the pH transition to this range is thought to be critical because escape from early endosomes is believed to be necessary for avoiding both drug exocytosis through early recycling endosomes and degradation in lysosomes following cellular internalization.[48,49] Predictably, all polymers with pK_a values <6 induced smaller amounts of hemolysis at pH 5.6. Interestingly, the two polymers with pK_a values >7 did not induce hemolysis until pH 5.6, which could be attributed either to alkyl chains preferentially self-interacting rather than inserting into the cell membrane or to limited polymer water solubility.

All polymers were screened for cytotoxicity in A7r5 rat aortic vascular smooth muscle cells after 30 min of treatment in vitro followed by either 0 or 24 h post-treatment incubation (Figure S19). In both experimental setups, toxicity was only observed at the highest polymer concentration tested 500 μg/mL. Only the 50:50 AA:hexyl showed any viability loss (~70% viability) in the 0 h incubation protocol, while the 50:50 AA:hexyl and AA:octyl and 70:30 AA:hexyl and AA:octyl showed toxicity in the 24 h incubation protocol. In subsequent cell uptake and activity studies, a polymer dose of 100–200 μg/mL was used that maintained high cell viability to ensure that cytotoxicity did not confound results (Figure S19).

While hemolysis is a widely used, highly reproducible assay, it does not fully recapitulate the more complex endosomal membrane composition or biochemical microenvironment. We recently reported on yellow fluorescent protein-Galectin-8 (YFP-Gal8) and split luciferase-based reporter cell lines for direct visualization and high throughput screening of endosome disruption.[45,50,51] The Gal8 machinery serves as part of the innate immune system for detection of intracellular entry by viruses and bacteria.[52] Upon disruption of endosomal vesicles, cytosolic Gal8 binds to exposed glycans selectively localized on the inner endosomal membrane. This phenomenon enables visualization and measurement of endosome disruption by tracking of YFP-Gal8, characterized by YFP-Gal8 redistribution from dispersed throughout the cell in the normal state to punctate and concentrated onto disrupted endosomal vesicles.

To use this in-cell endosome disruption assay, we treated A7r5 vascular smooth muscle cells that stably express YFP-Gal8 with a subset of polymers predicted to be endosomolytic based on red blood cell hemolysis results (50:50 AA:hexyl, 50:50 AA:octyl, 70:30 AA:hexyl, or 70:30 AA:octyl) or with poly(acrylic acid) (p(AA)) as a solely anionic, nonhydrophobically grafted control polymer anticipated to be nonendosomolytic. We chose A7r5 cells as they have been validated in our previous work for studying intracellular polymer and peptide uptake[50] and are a relevant cell type in studies on vasoactive peptides.[32,47,53] Untreated or p(AA)-treated cells displayed the predicted diffuse cellular fluorescence, while the cells treated with our leading compositions displayed robust punctate fluorescence within 30 min (Figure 1C). The number of punctate Gal8-positive spots per cell (quantified in ImageJ using a particle counting algorithm) increased approximately 50-fold over both untreated cells and p(AA)-treated cells for 50:50 AA:hexyl, 50:50 AA:octyl, and 70:30 AA:octyl (Figure 1D) ($p < 0.0001$, $n = 10$). Images were thresholded to count punctae with intensity greater than 2 standard deviations above average background intensity to minimize false

positives. While some punctae were visible following treatment with 70:30 AA:hexyl, the total counts were not statistically significant ($p > 0.05$, $n = 10$), even though this polymer induced significant hemolysis. This result underscores the advantage of screening polymers using the Gal8 assay in addition to red blood cell hemolysis, as the hemolysis assay does not completely recapitulate the intracellular endosomal environment. Since 70:30 AA:hexyl was the most hydrophilic polymer tested, we concluded that it likely had the lowest capacity for membrane interaction and intracellular pH-dependent endosome disruption. To further verify that the observation of Gal8-YFP puncta detection was due to pH-dependent, polymer-mediated endosome disruption, we cotreated cells with the polymer and Bafilomycin A (BafA), an inhibitor of endosome acidification. Accordingly, we observed no significant Gal8 recruitment relative to untreated cells ($p > 0.05$, $n = 10$) (Figure S20). These data demonstrate that a subset of polymers (50:50 AA:hexyl, 50:50 AA:octyl, and 70:30 AA:octyl) are capable of rapidly inducing endosomal disruption and that some degree of polymer internalization occurs during polymer-alone treatment. Polymer internalization was confirmed via flow cytometry by treating A7r5 cells with AlexaFluor-488 (A488)-labeled polymers for 30 min (Figure S21). We observed no significant uptake of p(AA), and a monotonic increase in cellular fluorescence as a function of alkyl length for all compositions, with only 50:50 AA:dodecyl breaking this trend, likely due to its low aqueous solubility, further validating that cell membrane translocation of these polymers is dependent on the hydrophobic content.

Next, we screened all 15 polymers for ability to promote intracellular delivery of cationic CPP. We and others have previously demonstrated the efficacy of a MAPKAP kinase II inhibitor peptide modified with the YARA cell-penetrating sequence (YARAAARQARA-KALARQLGVAA,[54] abbreviated YARA-MK2i). Efficient delivery of YARA-MK2i can inhibit inflammatory cytokine production, reduce vascular smooth muscle cell migration, and be used as an intra-operatively delivered prophylactic to reduce intimal hyperplasia and failure of autologous vein vascular grafts.[32,47] Herein, we used Alexa 488-labeled YARA-MK2i as a model cationic peptide to screen peptide internalization in vitro by flow cytometry following cell surface premodification with the candidate polymers. A7r5 cells were treated with each polymer for 30 min, then treated with 10 μM peptide in fresh media for 30 min, washed with DMEM containing 10% FBS to remove the surface-bound polymer and peptide, and immediately assayed for intracellular mean fluorescence intensity (MFI) relative to peptide treatment alone. By dosing the polymer and peptide separately and sequentially, we can elucidate the effect of the polymers as potentiators of CPP-cell surface interactions and more clearly probe the role of the polymer structure in cell–polymer and polymer–peptide interactions. The 10 μM peptide dose is nontoxic (Figure S19–G), and treatment with this dose using endosomolytic polymers was previously demonstrated to have a robust bioactive response in vitro.[47,53] Polymer treatment enhanced uptake of MK2i containing the YARA CPP by ~50% for 50:50 AA:hexyl and AA:octyl and by ~100% for 70:30 AA:octyl using a 5:1 mass ratio of polymer/peptide ([polymer] = 112 μg/mL) and a 10 μM peptide dose for all treatments (Figure 2A). Notably, the polymers that robustly potentiated peptide uptake also induced endosomal disruption as described above, while the nonendosomolytic polymers induced no significant enhancement of uptake relative to peptide alone.

We next tested the uptake of an MK2i peptide variant containing the more cationic oligoarginine CPP R6 rather than YARA (Figure 2B). Relative to the YARA-based peptide, the R6 CPP version achieved significantly greater potentiation of cell uptake from polymer pretreatment, with 50:50 AA:hexyl demonstrating a 13-fold increase in uptake and 50:50 AA:octyl, 70:30 AA:hexyl, and AA:octyl generating 4-fold, 5-fold, and 8-fold increase in uptake, respectively. Interestingly, several nonendosomolytic polymers increased uptake between 2 and 4-fold, including all AA:dodecyl polymers and several 90:10 AA:alkyl polymers that did not affect uptake for YARA-MK2i, suggesting that polymer-based, cell-peptide "baiting" could also be achieved independent of endosome-disrupting systems for application where endolysosomal compartment delivery is desirable. The 90:10 alkyl series may also only undergo a degree of membrane anchoring that can promote peptide–polymer interactions for the densely cationic R6-MK2i but is insufficient to enhance internalization of YARA-MK2i. For both CPPs, treatment with p(AA) failed to enhance uptake relative to peptide alone, which reinforces the hypothesis that hydrophobic interactions between the polymer and cell membrane is the critical first step of surface functionalization and ultimately the driver for increased peptide uptake.

We more thoroughly explored the impact of polymer concentration on subsequent peptide internalization using 70:30 AA/octyl due to its low toxicity and ability to enhance uptake of both YARA and R6-MK2i. Peptide concentration was held constant in this study, and the polymer/peptide mass ratio was varied between 1:1 and 20:1 (correlating to a polymer treatment of 22.4–448 μg/mL for YARA-MK2i and 20.3–407 μg/mL for R6-MK2i). YARA-MK2i uptake was maximized at a 10:1 mass ratio (Figure 2C), while increasing the polymer/peptide mass ratio beyond 5:1 had a minimal effect on uptake for the R6-MK2i peptide (Figure 2D). These data suggest that polymer-mediated enhancement of peptide uptake saturates at a polymer concentration of ~100 to 200 μg/mL, which is below where cytotoxicity becomes apparent (Figure S19). This could be due to cell surface saturation in this concentration range or because polymers preferentially self-associate and aggregate through hydrophobic interactions at higher concentrations rather than associate with the cell membrane. In support of the latter possibility, a decrease in cellular peptide uptake was observed at the highest polymer dose (Figure 2C, 448 μg/mL and Figure 2D, 406 μg/mL). Incubating polymers in a solution of Nile Red (a fluorophore that is selectively fluorescent only when partitioned into nonpolar environments) for 24 h produces a polymer composition-dependent increase in fluorescence at concentrations >100 μg/mL (Figure S22 and Table S1), indicating that significant hydrophobic aggregation occurs at higher concentrations that may limit the amount of unimeric polymer chains that can effectively associate with the cell surface.

Due to the striking difference in polymer-based potentiation of uptake between the two cationic CPP sequences, we expanded our investigation of peptide chemistry to include three additional CPPs that are widely utilized in therapeutic delivery. We screened one additional cationic, hydrophilic CPP, TAT, and two cationic, amphipathic CPPs: penetratin and transportan (Table S2). 50:50 AA:hexyl and 70:30 AA:octyl were selected to test uptake at a 5:1 polymer/peptide mass ratio and [peptide] = 10 μM, as these polymers and this mass ratio promoted the greatest enhancement of uptake for YARA- and R6-MK2i peptides. The amphipathic CPPs contain multiple hydrophobic domains and were selected to interrogate

whether combining ionic and hydrophobic polymer–peptide interactions could potentially further enhance uptake compared to purely ionic interactions. The 70:30 AA:octyl best potentiated uptake of the R6-MK2i, which was increased 7-fold, while 50:50 AA:hexyl increased uptake approximately 15-fold both for R6 and TAT-MK2i. Conversely, both polymers promoted only minimal uptake enhancement of penetratin and transportan-MK2i (Figure 3A–C). Plotting relative uptake against peptide charge density (number of positive charges/total number of AA residues; Figure 3D,E) or peptide isoelectric point at pH 7 (Figure 3F,G) reveals a general trend in polymer-driven increase in uptake as a function of increasing charge density and isoelectric point independent of the polymer structure. However, less clear is the trend in uptake as a function of total peptide charge, which is calculated as the total number of positive charges at pH 7, for either polymer treatment, with penetratin in particular falling outside of a potential trend (Figure 3H,I). These data further support the conclusion that relative differences in peptide uptake are driven by cooperative polymer–peptide interactions and suggest that, for the peptide, higher density of positive charge rather than total charge most significantly contributes to polymer-mediated potentiation of cellular uptake.

Our results to this point suggest that polymers associate with the cell membrane to enhance peptide uptake, as diagrammed in Figure 4A, with a strong dependence on both polymer and peptide chemistry. We visually confirmed this hypothesis using confocal microscopy (Figure 4B). A7r5 cells were loaded with Calcein Orange-Red AM dye to label the cytoplasm and treated with AlexaFluor-488-labeled polymers. We selected the four polymers 50:50 AA:hexyl, 50:50 AA:octyl, 70:30 AA:hexyl, and 70:30 AA:octyl for these experiments because they were found to best increase peptide uptake (Figure 2A,B). These polymers rapidly associated with the membrane after only a 5 min treatment, while there was no significant membrane association observed with p(AA). The more hydrophobic 50:50 AA:alkyl polymers exhibited some colocalization with the cytoplasmic dye, indicating rapid, partial cellular internalization, while the less hydrophobic 70:30 AA:alkyl polymers showed no observable cytoplasmic colocalization after 5 min. A representative slice from a z-stack reconstruction of each polymer treatment group further shows concentrated green fluorescence at the cell membrane that is not colocalized with cytosolic or nuclear staining (Figure 4C and Figure S23). The polymer coating, albeit somewhat heterogeneous and variable between polymers, covers the majority of the cell surface, especially for the three more hydrophobic polymers (50:50 AA:hexyl, 50:50 AA:octyl and 70:30 AA:octyl). Treating cells with 70:30 AA:hexyl, the least hydrophobic polymer among the subset tested, resulted in apparently less polymer–cell membrane association, consistent with our observation that this polymer candidate did not generate significant intracellular endosomal disruption or enhancement of peptide uptake. On the whole, this study demonstrates that a brief polymer pretreatment primes the cell surface with a hydrophobicity-driven coating that baits soluble, cationic CPPs.

Next, we sought to validate the mechanism by which polymer surface association potentiates intracellular peptide delivery. In addition to inert cell surface coating, polymer amphiphiles can induce lipid bilayer permeability through the formation of stable nanometer-scale pores[55–57] and ion-permeable channels,[58,59] which may serve as an additional mechanism for peptides to transduce the cell membrane as opposed to or in addition to enhancement

of endocytic uptake. We first examined whether treatment with the four lead candidate polymers permitted passive diffusion of higher molecular weight macromolecules into cells independent of electrostatic interactions with cationic cargo. A7r5 cells were incubated with FITC-dextran (M_n = 4000 or 40,000 g/mol) in the presence of 50:50 AA:hexyl, 50:50 AA:octyl, 70:30 AA:hexyl, or 70:30 AA:octyl polymers, and intracellular fluorescence was measured via flow cytometry after a 30 min treatment (Figure 5).

No significant increase in cell membrane permeability to dextran was observed as a function of polymer treatment. This result is also consistent with our hemolysis assay showing that hemoglobin does not pass through RBC membranes in the presence of these polymers at pH 7.4. It is therefore unlikely that our most membrane-interactive polymers are generating pores or otherwise disrupting the cell membrane sufficiently to permit extensive diffusion of peptides with a molecular weight of 2000–3000 g/mol as a primary mode of peptide cell membrane transduction. Observing that polymer treatment did not enable passive diffusion of macromolecules across the cell membrane provided further corroboration for our hypothesis that electrostatic binding between peptide and a hydrophobic/anionic polymer coating on the cell surface is the primary mechanism of inducing endocytic uptake with these CPP potentiators, as diagrammed in Figure 4A. This conclusion is also consistent with our demonstration of polymer-mediated, endosome acidification-dependent Gal8 recruitment to punctate vesicles as described above. To further elucidate the delivery mechanism, we performed a series of uptake experiments in the presence of a panel of endocytosis inhibitors (Figure S24 and supplemental discussion), which suggest that polymer-enhanced peptide uptake is driven by multiple endocytosis pathways that depend on both the polymer and peptide structure.

Finally, we verified that polymer-based cell surface modification could increase peptide intracellular bioavailability in vitro. We evaluated MK2i bioactivity in platelet-derived growth factor (PDGF)-stimulated A7r5 cells that we engineered to stably express cAMP response element-binding protein (CREB)-dependent transcriptional response elements in front of a CMV promoter for the luciferase gene (Figures S25 and S26). This is a useful test system for MK2i peptide bioactivity because under growth stimulation (PDGF), MK2 phosphorylates the CREB transcription factor, which drives migratory and proliferative phenotypes characteristic of the synthetic VSMC phenotype.[60–62] YARA-MK2i alone exhibited modest activity in this study, reducing luminescence by approximately 15%, compared to buffer control ($p < 0.05$) (Figure S26B). Polymer pretreatment significantly enhanced YARA-MK2i activity, with 70:30 AA:octyl reducing luminescence by 33% ($p < 0.05$). While this assay confirmed that our polymer treatments enhanced MK2i peptide activity, it exhibited a fairly low dynamic range and sensitivity in our hands. Furthermore, only partial MK2i-mediated CREB inhibition is expected because PDGF activation of CREB can proceed through both MK2-dependent and MK2-independent signaling pathways.[63,64]

The promising CREB study results motivated us to further explore polymer potentiation of peptide intracellular bioavailability by developing a new, more robust peptide bioactivity assay. To do so, we sought to derive a new peptide intracellular delivery assay with a high dynamic range and sensitivity based on the NanoLuc complementation technology that was

developed by Promega Corporation for intracellular protein quantification and assessment of protein–protein interactions.[65,66] The basis of this assay is the high affinity complementation of the small 11 amino acid peptide HiBiT (VSGWRLFKKIS) with a larger subunit of the NanoLuc enzyme known as LgBiT. LgBiT alone does not generate bioluminescence, but when complemented with the HiBiT peptide in the presence of the substrate furimazine, it creates bioluminescence that enables highly sensitive monitoring of molecular events over a large, linear dynamic range (Figure 6A).[67] A common implementation is to separately genetically fuse the HiBiT peptide and LgBiT domain to binding partners in the cell and then utilize NanoLuc signal to quantify protein–protein interactions. Our conceptualization of this assay is to exogenously deliver the CPP sequenced-fused HiBiT peptide to cells engineered to express the LgBiT domain, such that bioluminescence can be used to readout relative peptide delivery into cells.

Our NanoLuc implementation also integrated a strategy previously developed for virus-cell entry measurement in which a reporter was developed with LgBiT fused to the intracellular pleckstrin homology (PH) domain.[68] Fusion of LgBiT with the PH domain tethers the larger NanoLuc subunit stably within the cell and reduces assay background that can result from cellular release of LgBiT into the media.[69] We designed a new piggyBac vector with the LgBiT subunit and PH domain linked with a “GGGGS” triplet spacer (Figure S27). HEK-293 T cells were transfected with the piggyBac vector, and positively edited cells were selected with blasticidin. We confirmed that HEK-293 T cells engineered to stably express the LgBiT protein show dose-dependent luminescence in vitro when treated with an R6-HiBiT fusion peptide and Nano-Glo (furimazine) substrate (Figure S28). This new NanoLuc assay is rapid and highly sensitive to micromolar doses of peptide and serves as a valuable technique for high throughput screening of polymers or other approaches for intracellular peptide delivery.

We applied this assay to measure polymer-mediated delivery of the HiBiT peptide fused with YARA or R6. Pilot screens indicated that 50:50 AA:hexyl and 50:50 AA:octyl performed the best for intracellular bioactivity enhancement, so we thoroughly screened these lead polymers over a range of concentrations for sequential delivery of 1 μM YARA or R6-modified HiBiT peptide (Figure 6B). Polymer treatment produced a maximum dose-dependent enhancement in luminescence of up to 30-fold over peptide alone for 50:50 AA:hexyl + R6-HiBiT and 13-fold for 50:50 AA:octyl + R6-HiBiT. Both polymers were screened for cytotoxicity under similar treatment conditions in the engineered HEK-293 T cells (Figure 6C). The 50:50 AA:octyl polymer caused a slight yet statistically significant decrease in viability ($p < 0.05$) when dosed sequentially with R6-HiBiT, though viability remained >90% across all doses. The 50:50 AA:hexyl polymer also caused a slight decrease in viability when dosed sequentially with both YARA and R6-HiBiT, though viability was >85% for all polymer doses except 200 μg/mL, where viability decreased to ≈75%. While the highest doses of 50:50 AA:hexyl induce some toxicity, these experiments reveal polymer compositions and doses that produce a > 10 fold increase in peptide bioactivity while maintaining >90% cell viability and demonstrate this assay’s potential as a robust platform for screening peptide-delivery reagent formulations. In a parallel experiment, we tested for potentiation of peptide delivery using the previously established benchmark pyrene butyrate; however, this reagent produced at best a 1.3-fold increase in activity over peptide alone

(Figure S29) when applied using concentrations and incubation times optimized in previous literature reports.[22,23] These studies reported activity enhancement in the range of 1.5–5 fold at best, and uptake was proven to be an endocytic pathway with significant endosome entrapment. Pyrene butyrate also induced substantial cytotoxicity in our hands at 100 μM (29 μg/mL) and 200 μM (58 μg/mL), with viability decreasing to 65 and 57% respectively.

CONCLUSIONS

In summary, we have demonstrated the ability to modify the cell surface with anionic copolymers containing precisely tuned length and density of aliphatic alkyl side chains. A subset of these polymers containing 30 or 50 mol % of alkyl chains with 6 or 8 carbons in length exhibited pH-dependent membrane disruption that robustly induced endosomal escape as measured by hemolysis and an in vitro Gal8 reporter cell line. These same polymers enhanced intracellular delivery of a cationic peptide as a function of both polymer structure and identity of CPP present in the peptide through a mechanism driven by enhanced endocytosis, rather than passive diffusion due to physical membrane disruption. Enhancement of uptake was the greatest for peptides containing hydrophilic CPPs with high charge density, while polymer pretreatment was generally ineffective for delivering amphipathic CPPs containing more hydrophobic residues. The combined effects of polymeric hydrophobic moieties to promote lipid bilayer interaction, anionic carboxylates to electrostatically attract cationic peptides, and polymer pH-dependent endosome disruption enhanced CPP-modified intracellular model peptide bioavailability by up to 30-fold in a newly developed in vitro split-NanoLuc assay. The effective polymer dose across all assays was significantly below cytotoxic levels, indicating that polymer pretreatment robustly enhances peptide bioactivity in vitro without deleterious effects on cell viability. This sequential dosing approach has a substantial value toward enhancing the bioactivity of charged biomacromolecules through a simple, short-term polymer pretreatment, and our library of polymer formulations contributes new insights toward new materials for overcoming delivery barriers for a wide variety of intracellular therapeutic targets.

MATERIALS AND METHODS

Materials.

Dichloromethane (DCM, anhydrous, 99.8%), 1,4-dioxane (anhydrous, 99.8%), dimethylformamide (DMF, 99.8%, anhydrous), acryloyl chloride (97%), triethylamine (TEA, 99%), trifluoroacetic acid (TFA, 99%), tert-butyl acrylate (tBA, 98%), dimethylsulfoxide (DMSO, 99%), azobisisobutyronitrile (AIBN, 98%), 2,2′-dipyridyl disulfide (98%), FITC-dextran (4000, 40,000 g/mol), 1-pyrenebutyric acid (97%) Nile red, wortmannin (>98%), dynasore hydrate, methyl-β-cyclodextrin, and aluminum oxide (activated basic) were received from Sigma-Aldrich. Pentafluorophenol (99%) was received from Oakwood Chemical. *N*-propylamine (99%), *n*-butylamine (99%), *n*-hexylamine (99%), *n*-octylamine (99%), *n*-dodecylamine (99%), diethyl ether (anhydrous, 99%), acetone (99%), methanol (99%), hydrochloric acid solution (certified 0.0995–0.1005 N), and sodium hydroxide solution (certified 0.0995–0.1005 N) were received from Fisher Scientific. All MK2i and HiBiT peptide derivatives were received from EZBiolab. Bafilomycin A

(BafA) was received from Invivogen. Calcein Orange-Red AM, DAPI, AlexaFluor-488-N-hydroxysuccinimidyl (NHS) ester, and AlexaFluor-488-NH_2 were received from Thermo-Fisher Scientific. Anisole (99%) was received from Acros. Deuterated chloroform and deuterated methanol were received from Cambridge Isotope Laboratories. Dialysis tubing (3500 MWCO) was received from Spectrum Labs. PD-10 desalting columns containing Sephadex G-25 resin were received from GE Healthcare. tBA was distilled under reduced pressure and filtered once over basic alumina; AIBN was recrystallized from methanol, and all other chemicals were used as received. Ethyl cyanovaleric trithiocarbonate (ECT) was synthesized as previously described.[44]

Monomer Synthesis.

Pentafluorophenol (10 g, 0.054 mol) was dissolved in anhydrous DCM to a final concentration of 10% (w/v), and TEA (6.0 g, 0.06 mol) was slowly added. The reaction vessel was cooled to 0 °C, and a solution of acryloyl chloride (5.4 g, 0.06 mol) in anhydrous DCM (20% v/v) was added dropwise. The reaction mixture was stirred at room temperature overnight, and the TEA-HCl salt was filtered. The crude product was concentrated under reduced pressure and distilled under reduced pressure to afford PFPA (9.6 g, 75% yield). ^{1}H NMR (400 MHz, $CDCl_3$): δ 6.73 (dd, 1H), 6.37 (m, 1H), 6.18 (dd, 1H). ^{19}F NMR (500 MHz, $CDCl_3$): δ −150.9, (d, 2F), −156.2 (t, 1F), −160.7 (t, 2F).

Polymer Synthesis.

The poly(tBA-co-PFPA) parent polymers were synthesized via RAFT polymerization. Monomers were combined at a 50:50, 70:30, or 90:10 ratio (mol/mol) of tBA/PFPA in a round bottom flask and dissolved in dioxane (40% w/w). ECT and AIBN were added such that the total ratio of monomer/CTA/initiator was 200:1:0.2. The reaction mixture was purged with nitrogen for 30 min and transferred to a 65 °C oil bath for 24 h. The crude polymer was diluted with acetone, transferred to a dialysis membrane, and dialyzed against acetone for 48 h with three solvent exchanges every 24 h. The product was dried under reduced pressure to afford poly(tBA-co-PFPA). Each polymer batch of a given composition was split into five portions for alkylamine grafting. In general, a given polymer batch was dissolved in DMF (10% w/v) with a 2-fold molar excess of a given alkylamine and a 2-fold molar excess of pyridyl disulfide to cap thiols generated from aminolysis of the chain-end trithiocarbonate. For fluorescently labeled polymers, a solution of AlexaFluor-488-NH_2 dissolved in minimal DMSO was added at a target ratio of 1 fluorophore per polymer. The reaction was stirred overnight, dialyzed against acetone for 24 h with three solvent exchanges, and dried under reduced pressure. Each polymer was stirred overnight in a solution of 1:1 DCM/methanol containing 10% TFA (v/v) and 1% anisole (v/v) to convert tBA to acrylic acid (AA). The reaction mixture was precipitated 3× into cold diethyl ether and dried under reduced pressure. Stock solutions of each polymer were prepared at 20 mg/mL in 0.1 M NaOH and diluted in pH 8.0 phosphate buffer (10 mM) to given concentrations where indicated.

Materials Characterization.

Monomer and polymer structures were determined using ^{1}H NMR (Bruker, 400 MHz) and ^{19}F NMR (Bruker, 500 MHz). Polymer absolute molecular weight was determined using

gel permeation chromatography (GPC, Agilent Technologies) with 0.1% LiBr in DMF as the mobile phase with an inline refractive index detector (Agilent) and light scattering detector (Wyatt miniDAWN TREOS). Polymer pKa was measured using a Metrohm Titrino with automatic half-neutralization point calculation. Polymers were dissolved in 0.1 N NaOH (5 mg/mL) and titrated to the acid endpoint with 0.1 N HCl in 100 μL increments. Hydrophobic aggregation was measured using a modified critical micelle concentration assay as previously described.[70] Briefly, polymers were diluted in pH 8 phosphate buffer (10 mM) at given concentrations. A stock solution of Nile red in methanol (1 mg/mL) was added such that the final concentration was 0.01 mg/mL per sample. Samples were stored at room temperature in the dark for 24 h, and the Nile red fluorescence was read at 612 nm using a plate reader.

Hemolysis Assay.

The red blood cell assay was conducted as previously described.[46] Briefly, whole human blood was obtained from an anonymous donor, and the isolated red blood cells were incubated with the polymer at a given concentration and pH at 37 °C for 60 min. The cellular debris was centrifuged, and the absorbance of the released hemoglobin in the supernatant was measured at 405 nm. Percent hemolysis was calculated using PBS as a negative control for 0% hemolysis and Triton X-100 as a positive control for 100% hemolysis.

Cell Culture.

Rat aorta vascular smooth muscle cells (A7r5) were received from ATCC and cultured in Dulbecco's Modified Eagle's Medium (DMEM, Gibco) supplemented with 10% FBS (Gibco) and 1% penicillin/streptomycin (P/S, Invivogen) at 37 °C and 5% CO_2. Cells were passaged at 80–90% confluence, and the medium was refreshed every 2–3 days. All in vitro experiments were conducted on cells below passage number 10.

Cell Viability Assay.

Cells were seeded in a 96-well plate at 7500 cells/well and allowed to adhere overnight. The medium was replaced with OptiMEM (Gibco) supplemented with 1% FBS and 1% P/S at least 1 h before treatment. A given polymer solution (10 μL) in pH 8.0 phosphate buffer (10 mM) at 20× the final concentration was diluted in 190 μL of media, and the cells were incubated for 30 min. Cell viability was measured using the CellTiter-Glo assay (Promega) according to the manufacturer's protocol, which detects exogenous ATP as a measure of cell death. Briefly, 100 μL of supernatant was transferred to a well plate, and 100 μL of CellTiter-Glo reagent was added. The remaining media were aspirated, the cells were lysed with 100 μL of Triton X-100 (2% v/v), and 100 μL of CellTiter-Glo reagent was added. Cell viability was calculated as the luminescence from the retained ATP divided by total (retained + extracellular) ATP.

Confocal Microscopy.

Gal-8 Recruitment Assay.—YFP-Gal8 positive A7r5 cells were transduced as previously described.[50] Cells were seeded in 8-chamber coverslips at 2500 cells/well and allowed to

adhere for 48 h. Polymer treatments were applied to cells at a final concentration of 100 μg/mL in OptiMEM containing 1% FBS and 1% P/S, incubated for 30 min at 37 °C and 5% CO_2, and immediately imaged via confocal microscopy (Nikon Eclipse Ti). Cells receiving Bafilomycin A (BafA) were first treated with 100 nM BafA in PBS immediately before adding polymer treatments. The number of Gal8-positive punctae per cell was determined using the particle counting algorithm in ImageJ.

Confocal Imaging of Fluorescent Polymers.—A7r5 cells were seeded in 8-chamber coverslips at 2000 cells/well and allowed to adhere for 48 h. Cells were treated with 10 μM DAPI and 10 μM Calcein Orange-Red AM in OptiMEM containing 1% FBS and 1 %P/S for 30 min at 37 °C and 5% CO_2. After 30 min, the cells were gently washed with warm media and incubated in fresh media for 30 min. Fluorescent polymer treatments were applied at a final concentration of 100 μg/mL in OptiMEM containing 1% FBS and 1 %P/S. Images were acquired after 5 min of polymer treatment.

Flow Cytometry Uptake Assay.

Cells were seeded at 60,000 cells/well in a 12-well plate and allowed to adhere overnight. The medium was replaced with OptiMEM (Gibco) supplemented with 1% FBS and 1% P/S at least 1 h before treatment. A given polymer solution (50 μL) in pH 8.0 phosphate buffer (10 mM) was added in a 500 μL total volume, and the cells were incubated for a given duration. The medium was aspirated, and fresh, pre-equilibrated OptiMEM was applied. AlexaFluor-488-labeled YARA-MK2i or R6-MK2i (50 μL) was added for a final concentration of 10 μM in 500 μL total volume, and the cells were incubated for an additional 30 min. The medium was removed, and the cells were washed once with a warm complete growth medium and twice with PBS −/−. For endocytosis inhibitor studies, cells were pretreated with wortmannin (100 nM), dynasore hydrate (100 μM), or methyl-β-cyclodextrin (5 mM) for 30 min in OptiMEM with 1% FBS, 1% P/S. Fluorescently labeled polymer or peptide solutions were then added and cotreated with the inhibitor for 30 min. For polymer–peptide sequential treatments, polymer was cotreated with the inhibitor for 30 min, the medium was replaced with fresh OptiMEM, and fluorescently labeled peptide solutions were added (without inhibitors). Cells were harvested using 0.25% trypsin (Gibco), centrifuged, and resuspended in PBS −/− with 0.1% FBS (v/v). Uptake was quantified by flow cytometry (BD LSRII) as the mean intracellular fluorescence of 10,000 cells/sample.

Membrane Permeability Assay.

Membrane permeability was evaluated by measuring intracellular FITC-dextran uptake. A7r5 cells were seeded in a 12-well plate at 60,000 cells/well and allowed to adhere overnight. A given polymer solution (50 μL) in pH 8.0 phosphate buffer (10 mM) was added in a 500 μL total volume of OptiMEM containing 1% FBS and 1% P/S for a final polymer concentration of 100 μg/mL, along with FITC-dextran with indicated molecular weight at 10 μg/mL, and incubated for 30 min at 37 °C and 5% CO_2. Intracellular fluorescence was immediately measured using flow cytometry.

Peptide Synthesis.

Fluorecently labeled MK2i derivatives were synthesized by reacting each peptide with a 3-fold molar excess of Alexafluor-488-NHS in a 4:1 solution of DMSO/100 mM sodium bicarbonate buffer (pH 8.3) for 4 h at room temperature in the dark. Excess fluorophore and DMSO were removed using PD-10 desalting columns, and the product was lyophilized and stored at −20 °C.

YARA-MK2i Activity in Vitro Via the CREB-Luc A7r5 Cell Line.

Generation of the CREB-Luc Positive A7r5 Cell Line.—For viral production, HEK-293T cells were plated in a T75 flask and grown to ~50% confluence. VSV-G-expressing envelope plasmid pCMV-VSV-G (1 μg), psPAX2 packaging plasmid (10 μg), and pGF-CREB-mCMV-EF1 α-puro plasmid (10 μg) encoding dscGFP and luciferase in response to a cyclic AMP response element binding (CREB) protein activity at CREB transcriptional response elements (TREs) were transfected into cells utilizing the FuGENE 6 transfection reagent (Promega) in DMEM with 5% FBS (no antibiotics). Twenty-four hours later, the treatment was removed and replaced with a fresh medium. Fifty-six hours later, the supernatant was collected, centrifuged @ 2000 × g for 10 min, and syringe filtered through a 0.45 μm PTFE filter. The viral supernatant was stored at −80 °C until further use. A7r5 cells stably expressing luciferase downstream from a CREB TRE were generated by transduction with lentivirus diluted 1:2 in DMEM with 10% FBS and 8 μg/ml polybrene infection reagent (EMD Millipore) for 24 h. During the first 30 min of viral transduction, cells were spinoculated at 2000 rpm and then subsequently transferred to a cell culture incubator. After 24 h, viral treatments were removed and the cells were incubated in a fresh medium for an additional 24 h. Cells were then selected over a 10 day period with escalating doses of puromycin (2.5–15 μg/mL). Selected cells were then harvested and stored in cryovials with a freezing medium (10% DMSO in FBS) in a liquid nitrogen cell cryotank until further use.

MK2i Bioactivity Screen.—CREB-luc positive cells were plated at 10,000 cells/well in a black-walled 96-well plate and allowed to adhere overnight. A given polymer solution (10 μL) in pH 8.0 phosphate buffer (10 mM) was added to 90 μL of OptiMEM containing 1% FBS and 1% P/S for a final concentration of 10 μg/mL. Polymer treatment was performed for 30 min followed by 100 μM YARA-MK2i for 2 h. Control experiments were performed with 100 μM YARA-MK2i alone for 2h, or with the polymer alone for 30 min. The cells were carefully washed once with DMEM containing 10% FBS and stimulated with 20 ng/mL platelet-derived growth factor (PDGF, Peprotech) in DMEM containing 10% FBS for 18 h. The PDGF was removed, cells were treated with 150 μg/mL D-luciferin (Promega) in PBS, and luminescence intensity was measured using an IVIS imaging system (PerkinElmer). Luminescence was quantified relative to unstimulated cells, and polymer+peptide treatment groups were further normalized to polymer-only treatments. All statistics were calculated for $n = 4$ replicates.

Nanoluc Activity Assay.

Generation of the PH-LgBiT HEK 293 T Cell Line.—For Nanoluc cell line generation, a PH-LgBiT piggyBac vector was made by VectorBuilder (Figure S27). HEK

293 T cells were seeded into a 6 well plate at a density of 20,000 cells/well in DMEM supplemented with 10% serum and allowed to grow to 80% confluence. For transfection, 4 μg of the PH-LgBiT piggyBac vector, 4 μg of piggyBac transposase, and 10 μL of Lipofectamine 2000 (Invitrogen) were added on top of the cells. After incubating for 24 h post-transfection, the medium was removed and changed to fresh DMEM with 10% serum. After another 24 h, cell selection was initiated by replacing the medium with DMEM supplemented with 10% serum and 5 μg/mL blasticidin. Cells were passaged again once they reached 80% confluency.

Nanoluc Activity Screen.—HEK PH-LgBiT cells were seeded into 96-well plates at a density of 20,000 cells/well and allowed to adhere for 48 h. Once sufficiently confluent, the medium was replaced with high glucose DMEM supplemented with 1% FBS, 1% pen-strep, and 25 mM HEPES, and the cells were incubated for 30 min to acclimate. Then, the medium was removed, and the cells were dosed with polymer solutions in pH 8.0 phosphate buffer (10 mM) for final concentrations of 200, 150, 100, 50, 25, or 0 μg/mL of polymer in 1% serum DMEM with P/Sand HEPES buffer. The cells were incubated for another 30 min, and then, the medium was removed. The cells were then treated with 1 μM of either YARA-HiBiT (YARAAARQARA-VSGWRLFKKIS) or R6-HiBiT (RRRRRR-VSGWRLFKKIS) peptide in the same type of medium and incubated for another 30 min. Cells receiving pyrene butyrate (PyB) treatment during this step were incubated in PBS with PyB for 5 min before adding 1 uM YARA-HiBiT or R6-HiBiT so that the final PyB concentration was 200, 150, 100, 50, or 25 μM. The medium was removed and replaced with DMEM supplemented with 10% serum, 1% pen-strep, and 25 mM HEPES buffer. The cells were incubated for another 2 h before the addition of the Promega NanoGlo Live Cell Assay substrate. The luminescence of the cells was immediately measured using a TECAN Infinite M1000 Pro plate reader in a kinetic cycle for 20 min. Peak luminescence values were calculated by taking the average of the five values at the peak of the kinetic curve.

Statistical Analysis.

Statistical analysis was conducted using oneway ANOVA and Tukey's posthoc test for multiple comparisons. Analyses were performed using GraphPad Prism (La Jolla, CA). Statistical significance was accepted for $p < 0.05$, and data are presented as mean ± standard deviation.

Supplementary Material

Refer to Web version on PubMed Central for supplementary material.

ACKNOWLEDGMENTS

All authors acknowledge funding from NIH/NHLBI award number R01HL122347. KVK and RBF acknowledge support from NSF GRFP. The authors gratefully acknowledge the Vanderbilt University Flow Cytometry Shared Resource, Scott Guelcher for access to instrumentation, and Richard D'Arcy for helpful discussion during manuscript preparation.

REFERENCES

(1). Stephan MT; Irvine DJ Enhancing Cell Therapies from the Outside in: Cell Surface Engineering Using Synthetic Nanomaterials. Nano Today 2011, 6, 309–325. [PubMed: 21826117]

(2). Teramura Y; Iwata H Cell Surface Modification with Polymers for Biomedical Studies. Soft Matter 2010, 6, 1081–1091.

(3). Kellam B; De Bank PA; Shakesheff KM Chemical Modification of Mammalian Cell Surfaces. Chem. Soc. Rev. 2003, 32, 327–337. [PubMed: 14671788]

(4). Zhao W; Teo GSL; Kumar N; Karp JM Chemistry and Material Science at the Cell Surface. Mater. Today 2010, 13, 14–21.

(5). Fakhrullin RF; Zamaleeva AI; Minullina RT; Konnova SA; Paunov VN Cyborg Cells: Functionalisation of Living Cells with Polymers and Nanomaterials. Chem. Soc. Rev. 2012, 41, 4189–4206. [PubMed: 22509497]

(6). Wilson JT; Krishnamurthy VR; Cui W; Qu Z; Chaikof EL Noncovalent Cell Surface Engineering with Cationic Graft Copolymers. J. Am. Chem. Soc. 2009, 131, 18228–18229. [PubMed: 19961173]

(7). Wilson JT; Cui W; Kozlovskaya V; Kharlampieva E; Pan D; Qu Z; Krishnamurthy VR; Mets J; Kumar V; Wen J; Song Y; Tsukruk VV; Chaikof EL Cell Surface Engineering with Polyelectrolyte Multilayer Thin Films. J. Am. Chem. Soc. 2011, 133, 7054–7064. [PubMed: 21491937]

(8). Krol S; Del Guerra S; Grupillo M; Diaspro A; Gliozzi A; Marchetti P Multilayer Nanoencapsulation. New Approach for Immune Protection of Human Pancreatic Islets. Nano Lett. 2006, 6, 1933–1939. [PubMed: 16968004]

(9). Chanana M; Gliozzi A; Diaspro A; Chodnevskaja I; Huewel S; Moskalenko V; Ulrichs K; Galla HJ; Krol S Interaction of Polyelectrolytes and Their Composites with Living Cells. Nano Lett. 2005, 5, 2605–2612. [PubMed: 16351223]

(10). Davis HE; Rosinski M; Morgan JR; Yarmush ML Charged Polymers Modulate Retrovirus Transduction via Membrane Charge Neutralization and Virus Aggregation. Biophys. J. 2004, 86, 1234–1242. [PubMed: 14747357]

(11). Davis HE; Morgan JR; Yarmush ML Polybrene Increases Retrovirus Gene Transfer Efficiency by Enhancing Receptor-Independent Virus Adsorption on Target Cell Membranes. Biophys. Chem. 2002, 97, 159–172. [PubMed: 12050007]

(12). Teramura Y; Iwata H Islet Encapsulation with Living Cells for Improvement of Biocompatibility. Biomaterials 2009, 30, 2270–2275. [PubMed: 19201021]

(13). Teramura Y; Iwata H Surface Modification of Islets with PEG-Lipid for Improvement of Graft Survival in Intraportal Transplantation. Transplantation 2009, 88, 624–630. [PubMed: 19741458]

(14). Totani T; Teramura Y; Iwata H Immobilization of Urokinase on the Islet Surface by Amphiphilic Poly (Vinyl Alcohol) That Carries Alkyl Side Chains. Biomaterials 2008, 29, 2878–2883. [PubMed: 18395793]

(15). Godula K; Umbel ML; Rabuka D; Botyanszki Z; Bertozzi CR; Parthasarathy R Control of the Molecular Orientation of Membrane-Anchored Biomimetic Glycopolymers. J. Am. Chem. Soc. 2009, 131, 10263–10268. [PubMed: 19580278]

(16). Rabuka D; Forstner MB; Groves JT; Bertozzi CR Noncovalent Cell Surface Engineering: Incorporation of Bioactive Synthetic Glycopolymers into Cellular Membranes. J. Am. Chem. Soc. 2008, 130, 5947–5953. [PubMed: 18402449]

(17). Duvall CL; Convertine AJ; Benoit DSW; Hoffman AS; Stayton PS Intracellular Delivery of a Proapoptotic Peptide via Conjugation to a RAFT Synthesized Endosomolytic Polymer. Mol. Pharmaceutics 2010, 7, 468–476.

(18). Belting M; Sandgren S; Wittrup A Nuclear Delivery of Macromolecules: Barriers and Carriers. Adv. Drug Delivery Rev 2005, 57, 505–527.

(19). LeCher JC; Nowak SJ; McMurry JL Breaking in and Busting out: Cell-Penetrating Peptides and the Endosomal Escape Problem. Biomol. Concepts 2017, 8, 1011–1141.

(20). Mandal D; Nasrolahi Shirazi A; Parang K Cell-Penetrating Homochiral Cyclic Peptides as Nuclear-Targeting Molecular Transporters. Angew. Chem., Int. Ed. 2011, 50, 9633–9637.

(21). Nischan N; Herce HD; Natale F; Bohlke N; Budisa N; Cardoso MC; Hackenberger CP R Covalent Attachment of Cyclic TAT Peptides to GFP Results in Protein Delivery into Live Cells with Immediate Bioavailability. Angew. Chem., Int. Ed. 2015, 54, 1950–1953.

(22). Takeuchi T; Kosuge M; Tadokoro A; Sugiura Y; Nishi M; Kawata M; Sakai N; Matile S; Futaki S Direct and Rapid Cytosolic Delivery Using Cell-Penetrating Peptides Mediated by Pyrenebutyrate. ACS Chem. Biol 2006, 1, 299–303. [PubMed: 17163758]

(23). Guterstam P; Madani F; Hirose H; Takeuchi T; Futaki S; EL Andaloussi S; Gräslund A; Langel Ü Elucidating Cell-Penetrating Peptide Mechanisms of Action for Membrane Interaction, Cellular Uptake, and Translocation Utilizing the Hydrophobic Counter-Anion Pyrenebutyrate. Biochim. Biophys. Acta, Biomembr. 2009, 1788, 2509–2517.

(24). Perret F; Nishihara M; Takeuchi T; Futaki S; Lazar AN; Coleman AW; Sakai N; Matile S Anionic Fullerenes, Calixarenes, Coronenes, and Pyrenes as Activators of Oligo/Polyarginines in Model Membranes and Live Cells. J. Am. Chem. Soc. 2005, 127, 1114–1115. [PubMed: 15669846]

(25). Scherpereel A; Rome JJ; Wiewrodt R; Watkins SC; Harshaw DW; Alder S; Christofidou-Solomidou M; Haut E; Murciano JC; Nakada M; Albelda SM; Muzykantov VR Platelet-Endothelial Cell Adhesion Molecule-1-Directed Immunotargeting to Cardiopulmonary Vasculature. J. Pharmacol. Exp. Ther. 2002, 300, 777–786. [PubMed: 11861781]

(26). Danielyan K; Ding BS; Gottstein C; Cines DB; Muzykantov VR Delivery of Anti-Platelet-Endothelial Cell Adhesion Molecule Single-Chain Variable Fragment-Urokinase Fusion Protein to the Cerebral Vasculature Lyses Arterial Clots and Attenuates Postischemic Brain Edema. J. Pharmacol. Exp. Ther. 2007, 321, 947–952. [PubMed: 17389242]

(27). Muro S; Dziubla T; Qiu W; Leferovich J; Cui X; Berk E; Muzykantov VR Endothelial Targeting of High-Affinity Multivalent Polymer Nanocarriers Directed to Intercellular Adhesion Molecule 1. J. Pharmacol. Exp. Ther. 2006, 317, 1161–1169. [PubMed: 16505161]

(28). Garnacho C; Albelda SM; Muzykantov VR; Muro S Differential Intra-Endothelial Delivery of Polymer Nanocarriers Targeted to Distinct PECAM-1 Epitopes. J. Controlled Release 2008, 130, 226–233.

(29). Shuvaev VV; Muro S; Arguiri E; Khoshnejad M; Tliba S; Christofidou-Solomidou M; Muzykantov VR Size and Targeting to PECAM vs ICAM Control Endothelial Delivery, Internalization and Protective Effect of Multimolecular SOD Conjugates. J. Controlled Release 2016, 234, 115–123.

(30). Kozower BD; Christofidou-Solomidou M; Sweitzer TD; Muro S; Buerk DG; Solomides CC; Albelda SM; Patterson GA; Muzykantov VR Immunotargeting of Catalase to the Pulmonary Endothelium Alleviates Oxidative Stress and Reduces Acute Lung Transplantation Injury. Nat. Biotechnol. 2003, 21, 392–398. [PubMed: 12652312]

(31). Evans BC; Fletcher RB; Kilchrist KV; Dailing EA; Mukalel AJ; Colazo JM; Oliver M; Cheung-flynn J; Brophy CM; Tierney JW; Isenberg JS; Hankenson KD; Ghimire K; Lander C; Gersbach CA; Duvall CL An Anionic, Endosome-Escaping Polymer to Potentiate Intracellular Delivery of Cationic Peptides, Biomacromolecules, and Nanoparticles. Nat. Commun 2019, 10, 5012. [PubMed: 31676764]

(32). Evans BC; Hocking KM; Osgood MJ; Voskresensky I; Dmowska J; Kilchrist KV; Brophy CM; Duvall CL MK2 Inhibitory Peptide Delivered in Nanopolyplexes Prevents Vascular Graft Intimal Hyperplasia. Sci. Transl. Med 2015, 7, 291ra95.

(33). Udofot O; Lin L-H; Thiel WH; Erwin M; Turner E; Miller FJ; Giangrande PH; Yazdani SK Delivery of Cell-Specific Aptamers to the Arterial Wall with an Occlusion Perfusion Catheter. Mol. Ther. Nucleic Acids 2019, 16, 360–366. [PubMed: 30986697]

(34). Eberhardt M; Mruk R; Zentel R; Théato P Synthesis of Pentafluorophenyl (Meth) Acrylate Polymers: New Precursor Polymers for the Synthesis of Multifunctional Materials. Eur. Polym. J. 2005, 41, 1569–1575.

(35). Boyer C; Bulmus V; Davis TP; Ladmiral V; Liu J; Perrier S Bioapplications of RAFT Polymerization. Chem. Rev. 2009, 109, 5402–5436. [PubMed: 19764725]

(36). Vanderburgh J; Hill JL; Gupta MK; Kwakwa KA; Wang SK; Moyer K; Bedingfield SK; Merkel AR; D'Arcy R; Guelcher SA; Rhoades JA; Duvall CL Tuning Ligand Density To Optimize Pharmacokinetics of Targeted Nanoparticles for Dual Protection against Tumor-Induced Bone Destruction. ACS Nano 2020, 14, 311–327. [PubMed: 31894963]

(37). Beija M; Li Y; Lowe AB; Davis TP; Boyer C Factors Influencing the Synthesis and the Post-Modification of PEGylated Pentafluorophenyl Acrylate Containing Copolymers. Eur. Polym. J. 2013, 49, 3060–3071.

(38). Yessine MA; Leroux JCM-DP Interaction with Lipid Bilayers and Endosomal Escape of Biomacromolecules. Adv. Drug Delivery Rev 2004, 56, 999–1021.

(39). Murthy N; Robichaud JR; Tirrell DA; Stayton PS; Hoffman AS The Design and Synthesis of Polymers for Eukaryotic Membrane Disruption. J. Controlled Release 1999, 61, 137–143.

(40). Philippova OE; Hourdet D; Audebert R; Khokhlov AR PH-Responsive Gels of Hydrophobically Modified Poly (Acrylic Acid). Macromolecules 1997, 30, 8278–8285.

(41). Philippova OE; Hourdet D; Audebert R; Khokhlov AR Interaction of Hydrophobically Modified Poly (Acrylic Acid) Hydrogels with Ionic Surfactants. Macromolecules 1996, 29, 2822–2830.

(42). Sakaguchi N; Kojima C; Harada A; Kono K Preparation of PH-Sensitive Poly (Glycidol) Derivatives with Varying Hydrophobicities: Their Ability to Sensitize Stable Liposomes to PH. Bioconjugate Chem. 2008, 19, 1040–1048.

(43). Tonge SR; Tighe BJ Responsive Hydrophobically Associating Polymers: A Review of Structure and Properties. Adv. Drug Delivery Rev 2001, 53, 109–122.

(44). Nelson CE; Kintzing JR; Hanna A; Shannon JM; Gupta MK; Duvall CL Balancing Cationic and Hydrophobic Content of PEGylated SiRNA Polyplexes Enhances Endosome Escape, Stability, Blood Circulation Time, and Bioactivity in Vivo. ACS Nano 2013, 7, 8870–8880. [PubMed: 24041122]

(45). Kilchrist KV; Dimobi SC; Jackson MA; Evans BC; Werfel TA; Dailing EA; Bedingfield SK; Kelly IB; Duvall CL Gal 8 Visualization of Endosome Disruption Predicts Carrier-Mediated Biologic Drug Intracellular Bioavailability. ACS Nano 2019, 13, 1136–1152. [PubMed: 30629431]

(46). Evans BC; Nelson CE; Yu SS; Beavers KR; Kim AJ; Li H; Nelson HM; Giorgio TD; Duvall CL Ex Vivo Red Blood Cell Hemolysis Assay for the Evaluation of PH-Responsive Endosomolytic Agents for Cytosolic Delivery of Biomacromolecular Drugs. J. Visualized Exp 2013, 73, No. e50166.

(47). Evans BC; Hocking KM; Kilchrist KV; Wise ES; Brophy CM; Duvall CL Endosomolytic Nano-Polyplex Platform Technology for Cytosolic Peptide Delivery to Inhibit Pathological Vasoconstriction. ACS Nano 2015, 9, 5893–5907. [PubMed: 26004140]

(48). Varkouhi A; Scholte M; Storm G; Haisma H Endosomal Escape Pathways for Delivery of Biologicals. J. Controlled Release 2011, 151, 220–228.

(49). Sahay G; Querbes W; Alabi C; Eltoukhy A; Sarkar S; Zurenko C; Karagiannis E; Love K; Chen D; Zoncu R; Buganim Y; Schroeder A; Langer R; Anderson DG Efficiency of SiRNA Delivery by Lipid Nanoparticles Is Limited by Endocytic Recycling. Nat. Biotechnol. 2013, 31, 653–658. [PubMed: 23792629]

(50). Kilchrist KV; Evans BC; Brophy CM; Duvall CL Mechanism of Enhanced Cellular Uptake and Cytosolic Retention of MK2 Inhibitory Peptide Nano-Polyplexes. Cell. Mol. Bioeng 2016, 9, 368–381. [PubMed: 27818713]

(51). Kilchrist KV; Tierney JW; Duvall CL Genetically Encoded Split-Luciferase Biosensors to Measure Endosome Disruption Rapidly in Live Cells. ACS sensors 2020, 5, 1929–1936. [PubMed: 32573202]

(52). Thurston TLM; Wandel MP; Von Muhlinen N; Foeglein Á; Randow F Galectin 8 Targets Damaged Vesicles for Autophagy to Defend Cells against Bacterial Invasion. Nature 2012, 482, 414–418. [PubMed: 22246324]

(53). Mukalel AJ; Evans BC; Kilchrist KV; Dailing EA; Burdette B; Cheung-Flynn J; Brophy CM; Duvall CL Excipients for the Lyoprotection of MAPKAP Kinase 2 Inhibitory Peptide Nano-Polyplexes. J. Controlled Release 2018, 282, 110–119.

(54). Ward B; Seal BL; Brophy CM; Panitch A Design of a Bioactive Cell-Penetrating Peptide: When a Transduction Domain Does More than Transduce. J. Pept. Sci. 2009, 15, 668–674. [PubMed: 19691016]

(55). Vial F; Oukhaled AG; Auvray L; Tribet C Long-Living Channels of Well Defined Radius Opened in Lipid Bilayers by Polydisperse, Hydrophobically-Modified Polyacrylic Acids. Soft Matter 2007, 3, 75–78.

(56). Tribet C; Vial F Flexible Macromolecules Attached to Lipid Bilayers: Impact on Fluidity, Curvature, Permeability and Stability of the Membranes. Soft Matter 2008, 4, 68–81.

(57). Werner M; Sommer JU Translocation and Induced Permeability of Random Amphiphilic Copolymers Interacting with Lipid Bilayer Membranes. Biomacromolecules 2015, 16, 125–135. [PubMed: 25539014]

(58). Thomas JL; Barton SW; Tirrell DA Membrane Solubilization by a Hydrophobic Polyelectrolyte: Surface Activity and Membrane Binding. Biophys. J. 1994, 67, 1101–1106. [PubMed: 7811920]

(59). Chung JC; Gross DJ; Thomas JL; Tirrell DA; Opsahl-Ong LR PH-Sensitive, Cation-Selective Channels Formed by a Simple Synthetic Polyelectrolyte in Artificial Bilayer Membranes. Macromolecules 1996, 29, 4636–4641.

(60). Jalvy S; Renault MA; Leen LLS; Belloc I; Reynaud A; Gadeau AP; Desgranges C CREB Mediates UTP-Directed Arterial Smooth Muscle Cell Migration and Expression of the Chemotactic Protein Osteopontin via Its Interaction with Activator Protein-1 Sites. Circ. Res 2007, 100, 1292–1299. [PubMed: 17413042]

(61). Lee GL; Chang YW; Wu JY; Wu ML; Wu KK; Yet SF; Kuo CC TLR 2 Induces Vascular Smooth Muscle Cell Migration through CAMP Response Element-Binding Protein-Mediated Interleukin-6 Production. Arterioscler., Thromb., Vasc. Biol. 2012, 32, 2751–2760. [PubMed: 22995520]

(62). Nakanishi K; Saito Y; Azuma N; Sasajima T Cyclic Adenosine Monophosphate Response-Element Binding Protein Activation by Mitogen-Activated Protein Kinase-Activated Protein Kinase 3 and Four-and-a-Half LIM Domains 5 Plays a Key Role for Vein Graft Intimal Hyperplasia. J. Vasc. Surg. 2013, 57, 182–193.e10. [PubMed: 23127979]

(63). Egan CG; Wainwright CL; Wadsworth RM; Nixon GF PDGF-Induced Signaling in Proliferating and Differentiated Vascular Smooth Muscle: Effects of Altered Intracellular Ca2+ Regulation. Cardiovasc. Res 2005, 67, 308–316. [PubMed: 15885673]

(64). Koga Y; Tsurumaki H; Aoki-Saito H; Sato M; Yatomi M; Takehara K; Hisada T Roles of Cyclic AMP Response Element Binding Activation in the ERK1/2 and P 38 MAPK Signalling Pathway in Central Nervous System, Cardiovascular System, Osteoclast Differentiation and Mucin and Cytokine Production. Int. J. Mol. Sci 2019, 20, 1–23.

(65). White CW; Caspar B; Vanyai HK; Pfleger KDG; Hill SJ CRISPR-Mediated Protein Tagging with Nanoluciferase to Investigate Native Chemokine Receptor Function and Conformational Changes. Cell Chem. Biol 2020, 510.e7.

(66). Schwinn MK; Machleidt T; Zimmerman K; Eggers CT; Dixon AS; Hurst R; Hall MP; Encell LP; Binkowski BF; Wood KV CRISPR-Mediated Tagging of Endogenous Proteins with a Luminescent Peptide. ACS Chem. Biol 2018, 13, 467–474. [PubMed: 28892606]

(67). England CG; Ehlerding EB; Cai W Nano Luc: A Small Luciferase Is Brightening Up the Field of Bioluminescence. Bioconjugate Chem. 2016, 27, 1175–1187.

(68). Wang J; Kondo N; Long Y; Iwamoto A; Matsuda Z Monitoring of HIV-1 Envelope-Mediated Membrane Fusion Using Modified Split Green Fluorescent Proteins. J. Virol. Methods 2009, 161, 216–222. [PubMed: 19559731]

(69). Yamamoto M; Du Q; Song J; Wang H; Watanabe A; Tanaka Y; Kawaguchi Y; Inoue JI; Matsuda Z Cell Cell and Virus Cell Fusion Assay Based Analyses of Alanine Insertion Mutants in the Distal 9 Portion of the JRFL Gp41 Subunit from HIV-1. J. Biol. Chem. 2019, 294, 5677–5687. [PubMed: 30737278]

(70). Gupta MK; Meyer TA; Nelson CE; Duvall CL Poly (PS-b-DMA) Micelles for Reactive Oxygen Species Triggered Drug Release. J. Controlled Release 2012, 162, 591–598.

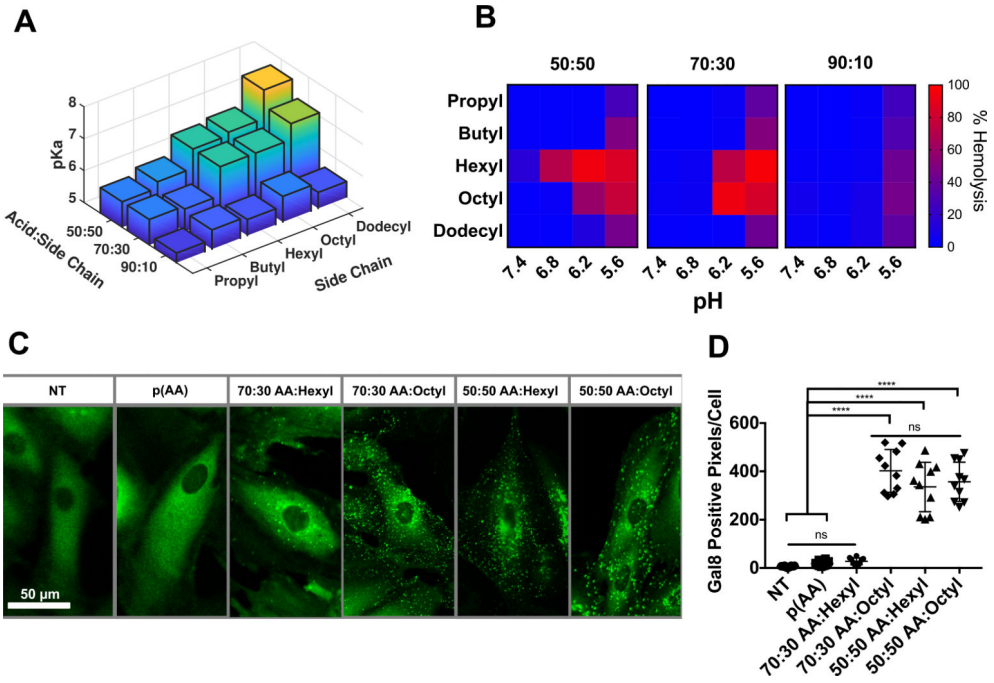

Figure 1.

Polymers with ideally tuned anionic and hydrophobic content induce pH-dependent membrane disruption. (A) Polymer pK_a as determined by acid–base titration. (B) Polymers were screened in a pH-dependent red blood cell hemolysis assay at 5 μg/mL as a gauge for cytocompatibility and endosome escape capability. (C) YFP-Gal8 reporter cells were treated with polymers at 100 μg/mL and imaged via confocal microscopy to visualize endosome disruption. (D) Gal8 recruitment into punctate spots was quantified via ImageJ ($n = 10$). **** = $p < 0.0001$, ns = $p > 0.05$.

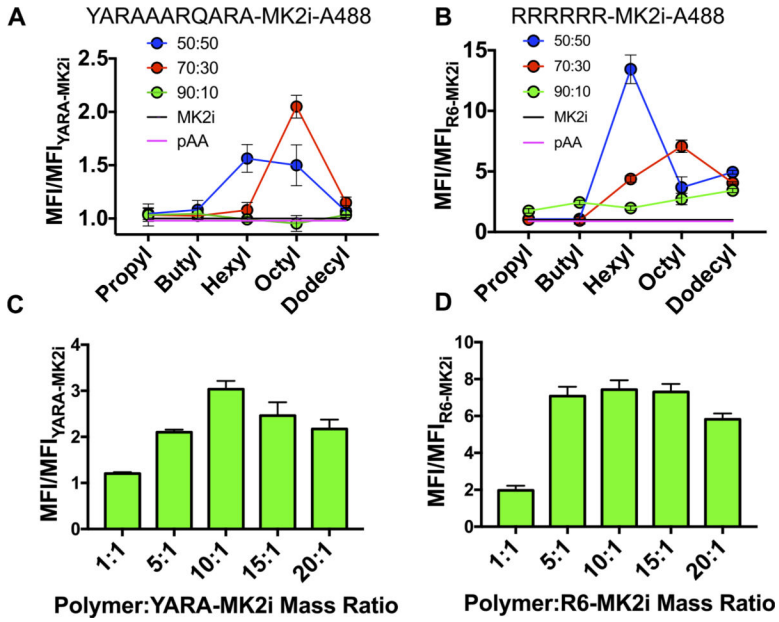

Figure 2.

Cell surface polymer premodification enhances peptide cellular uptake in vitro and is dependent on both the polymer structure and peptide cationic CPP sequence. Fold change in the mean fluorescence intensity of cells treated with polymers followed by AlexaFluor-488-modified (A) YARA-MK2i or (B) R6-MK2i in a 5:1 polymer/peptide mass ratio (n = 3). Fold change in the mean fluorescence intensity of cells treated with 70:30 AA:octyl followed by AlexaFluor-488-modified (C) YARA-MK2i or (D) R6-MK2i as a function of polymer/peptide mass ratio (n = 3).

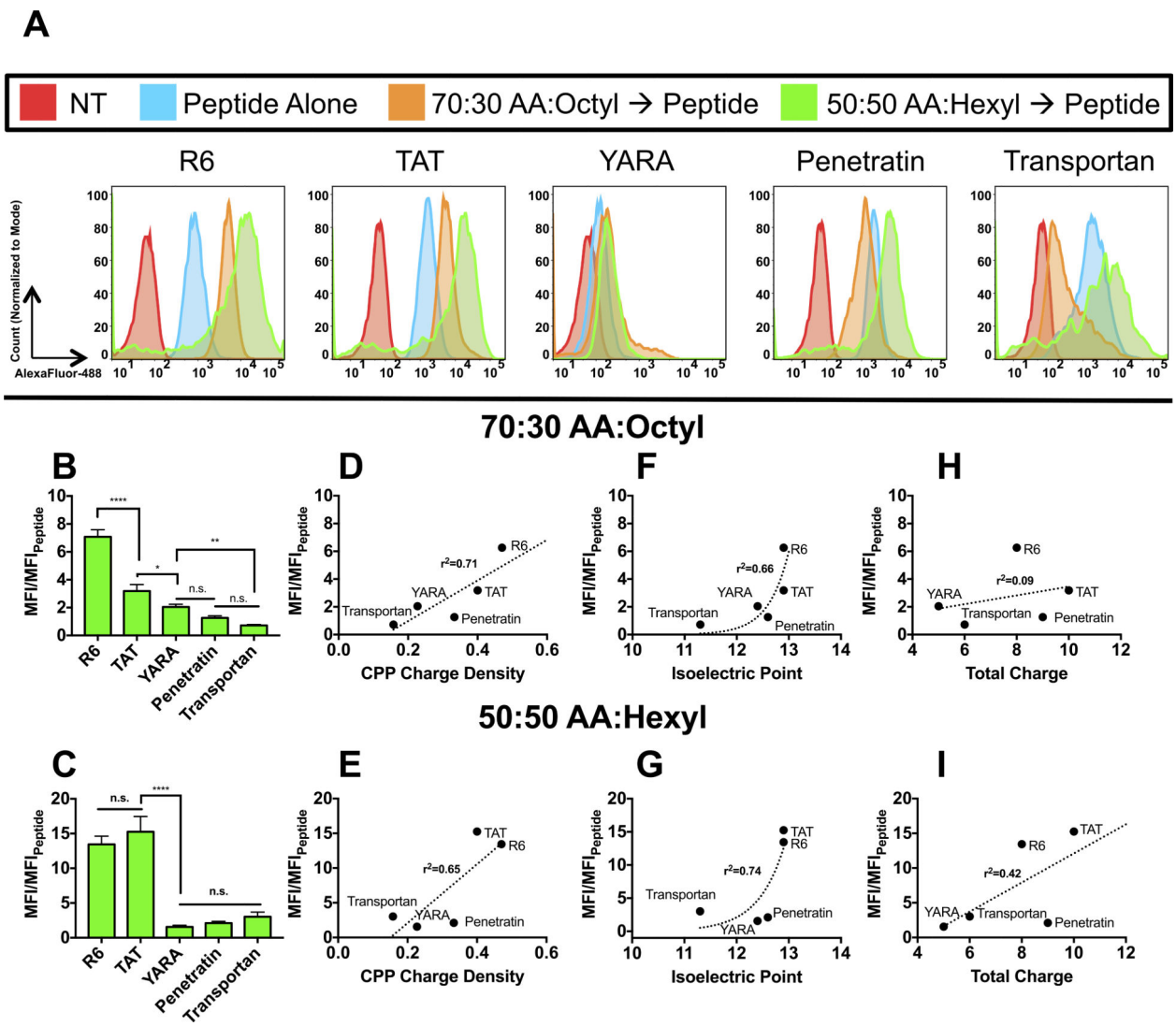

Figure 3.

Polymer pretreatment results in the greatest enhancement of uptake for peptides with densely cationic cell penetrating sequences. (A) Flow cytometry histograms of mean intracellular fluorescence following sequential treatment with indicated polymer and AlexaFluor-488-modified MK2i with indicated cationic CPP sequences. (B, C) Fold change in the mean fluorescence intensity of cells treated with polymers followed by AlexaFluor-488-modified MK2i with indicated cationic CPP sequences ($n = 3$). * = $p < 0.05$, ** = $p < 0.01$, *** = $p < 0.001$, **** = $p < 0.0001$. D–I) Peptide uptake plotted as a function of (D, E) CPP charge density (total charge at pH 7/# of AAs), (F, G) isoelectric point, and (H, I) total peptide charge (total # of cationic residues at pH 7).

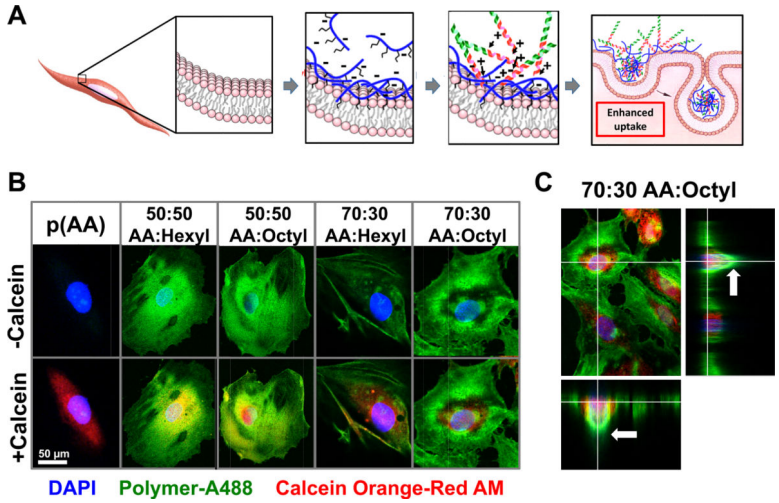

Figure 4.

Polymer hydrophobicity promotes cell membrane association. (A) Proposed mechanism for polymer-enhanced peptide uptake: polymers stably insert into the cell membrane through hydrophobic interactions and attract cationic peptides to the cell surface through electrostatic interactions. (B) Confocal microscopy of A7r5 cells treated with the AlexaFluor-488-labeled polymer for 5 min. Nuclei are stained with DAPI, and cytoplasm is loaded with Calcein Orange-Red. (C) Confocal z-slice with arrows indicating polymers associated with the cell membrane.

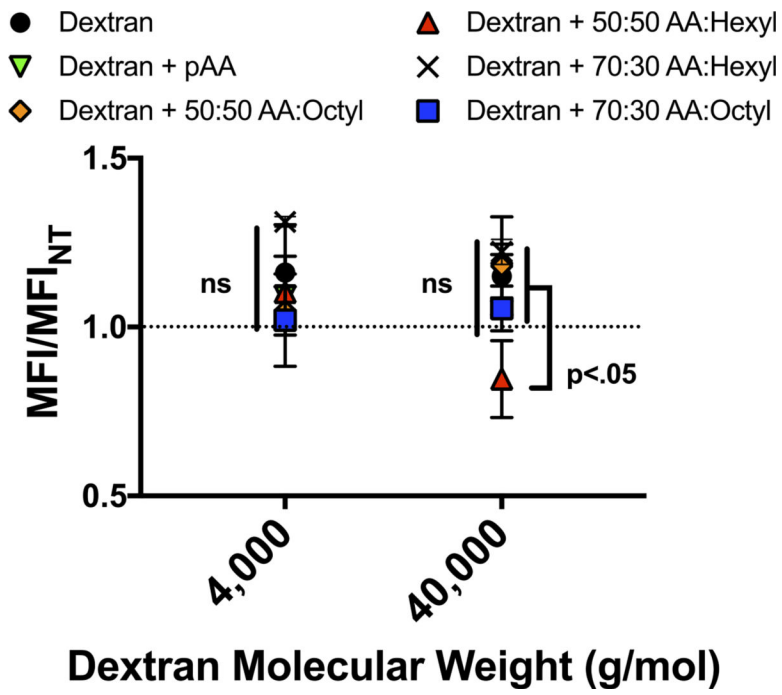

Figure 5.

Polymer–peptide interactions at the cell membrane do not induce passive diffusion into the cell by creating membrane leakiness. Fold change in the mean fluorescence intensity of A7r5 cells treated with FITC-Dextran and indicated polymers ($n = 3$, ns = $p > 0.05$).

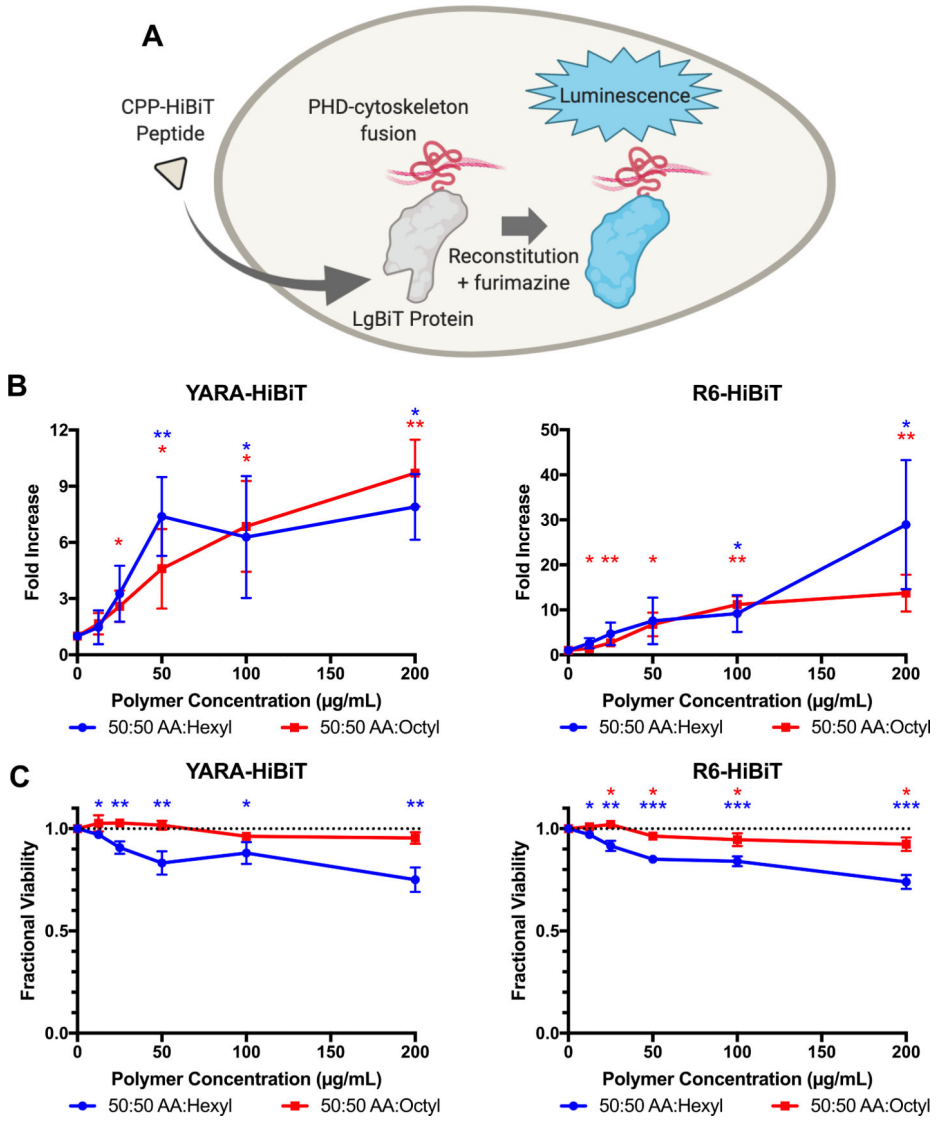

Figure 6.

Polymer pretreatment enhances the intracellular bioactivity of CPP-modified HiBiT peptide in the NanoLuc luminescence assay. (A) NanoLuc assay utilizes cells expressing the LgBiT domain genetically fused with a pleckstrin homology domain (PHD) to retain LgBiT onto the intracellular cytoskeleton, preventing false positives through extracellular secretion or leakage of LgBiT into the media. Cytosolic reconstitution between LgBiT and the CPP-modified HiBiT peptide produces a luminescence signal in the presence of the substrate. (B) Fold change in intracellular luminescence relative to peptide alone in HEK-293 T cells expressing LgBiT following sequential treatment with the indicated polymer and CPP-modified HiBiT peptide ($n = 4$). Individual markers above each point indicate significant signal enhancement relative to no polymer pretreatment. (C) Viability of HEK-293 T cells following polymer and peptide treatment ($n = 4$). Individual markers above each point indicate significant change in viability relative to PBS. * = $p < 0.05$, ** = $p < 0.01$, *** = $p < 0.001$.

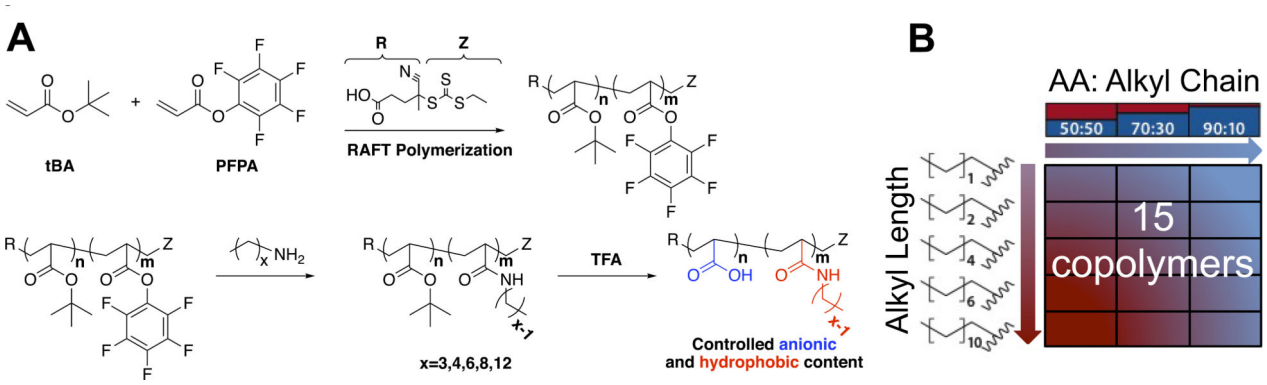

Scheme 1. Synthesis of a Polymer Library Containing Anionic Groups and Aliphatic Alkyl Side Chains with Highly Defined Length and Density[a]

[a] (A) A library of random copolymers of acrylic acid and alkyl acrylamides was synthesized via RAFT polymerization of t-butyl acrylate (tBA) and pentafluorophenyl acrylate (PFPA) and subsequent grafting of alkyl amines through the pentafluorophenyl ester. (B) A combinatorial library of 15 polymers with varying lengths and densities of alkyl side chains was prepared via controlling the comonomer ratio and alkyl amine structure. Color is illustrative of relative anionic (blue) and hydrophobic (red) content.

Table 1.

Polymer Composition, Molecular Weight, and Dispersity as Determined by ^{1}H NMR (a) and GPC (b)

monomer feed (tBA/PFPA)	product composition (tBA/PFPA)$_a$	M_n (g/mol)$_b$	$Đ_b$	alkyl groups/polymer$_a$	COOH/polymer$_a$
50:50	45:55	26,900	1.06	78	64
70:30	71:29	29,300	1.10	53	129
90:10	86:14	27,100	1.08	26	167